

DERIVING HIGH-RESOLUTION VELOCITY MAPS FROM LOW-RESOLUTION FOURIER VELOCITY ENCODED MRI DATA

V. C. Rispoli *

Engineering Faculty at Gama
University of Brasilia, Brazil
e-mail: vrispoli@pgea.unb.br

J. L. A. Carvalho

Department of Electrical Engineering
University of Brasilia, Brazil
e-mail: joaoluiz@pgea.unb.br

ABSTRACT

Fourier velocity encoding (FVE) is a promising magnetic resonance imaging (MRI) method for measurement of cardiovascular blood flow. FVE provides considerably higher SNR than phase contrast imaging, and is robust to partial-volume effects. FVE data is usually acquired with low spatial resolution, due to scan-time restrictions associated with its higher dimensionality. Thus, FVE is capable of providing the velocity distribution associated with a large voxel, but does not directly provides a velocity map. Velocity maps, however, are useful for calculating the actual blood flow through a vessel, or for guiding computational fluid dynamics simulations. This work proposes a method to derive velocity maps with high spatial resolution from low-resolution FVE data using a hyper-Laplacian prior deconvolution algorithm. Experiments using numerical phantoms, as well simulated spiral FVE data derived from real phase contrast data, acquired using a pulsatile carotid flow phantom, show that it is possible to obtain reasonably accurate velocities maps from low-resolution FVE distributions.

Index Terms— MRI; phase contrast; Fourier velocity encoding; FVE; blood flow; cardiovascular disease

1. INTRODUCTION

The current gold standard for MRI flow quantification is phase contrast (PC) [1]. However, PC suffers from partial-volume effects when a wide distribution of velocities is contained within a voxel [2]. Particularly, this is problematic when flow is turbulent and/or complex (e.g., flow jets due to stenosis), or at the interface between blood and vessel wall (viscous sublayer). This issue is typically addressed by increasing the spatial resolution, which dramatically affects the signal-to-noise ratio (SNR) and increases the scan time. Therefore, PC may be inadequate for estimating the peak velocity of stenotic flow jets, for example.

Fourier velocity encoded (FVE) MRI is an alternative to phase contrast imaging. FVE provides considerably higher

SNR than PC, due to its higher dimensionality and larger voxel sizes. Furthermore, FVE is robust to partial voluming, as it measures the velocity distribution within each voxel. This makes FVE particularly useful for assessment of flow jets due to stenosis [3]. Spiral FVE is a rapid method for FVE-based velocity-distribution measurement [3]. It consists in combining slice-selective spiral imaging along the spatial k -space (k_x - k_y) with phase-encoding along the velocity Fourier dimension (k_v).

FVE data is usually acquired with low spatial resolution, due to scan-time restrictions associated with its higher dimensionality. Thus, FVE is capable of providing the velocity distribution associated with a large voxel, but does not directly provides a velocity map. Velocity maps, however, are useful for calculating the actual blood flow through a vessel, or for guiding computational fluid dynamics simulations [4].

This work proposes a method to derive velocity maps with high spatial resolution from low-resolution FVE data. The proposed method is based on a mathematical model of the FVE distribution, $s(x, y, v)$, and involves deconvolving the low-resolution FVE velocity distribution kernel calculated based on the k_x - k_y coverage of the k -space trajectory of the FVE acquisition. Experiments using numerical phantoms, as well simulated spiral FVE data derived from real phase contrast data, acquired using a pulsatile carotid flow phantom, show that it is possible to obtain reasonably accurate velocities maps from low-resolution FVE data.

2. METHODOLOGY

A signal model that incorporates spiral FVE k -space truncation effects [5] (described below) was used to derive a procedure to determine a high-resolution velocity map from the low-resolution FVE data. This model shows that the FVE velocity distribution can be modeled from high-resolution velocity maps, using the blurring kernel associated with the k_x - k_y coverage of the k -space trajectory of the FVE acquisition. Thus, we propose deconvolving the measured spiral FVE data with this known blurring kernel. In order to estimate the velocity map, we compare the measured FVE velocity distribu-

*This work was supported by the University of Brasilia Research and Graduate Chamber (DPP/UnB).

tion, $s(v)$, to a sinc function, which models blurring along the velocity dimension due to finite coverage (truncation) of the velocity k -space (k_v). We will describe these steps in further detail next.

2.1. Spiral FVE signal model

Fourier velocity encode resolves the distribution of velocities $s(v)$ within each voxel by Fourier encoding along at least one velocity axis [6]. In this work, velocity (v) is encoded only along the through-plane axis (z), and the data are spatially resolved along two in-plane axes (x, y). The FVE signal measured at each cardiac phase is a three-dimensional function $s(x, y, v)$.

Standard phase contrast measurements provides two two-dimensional functions, $m(x, y)$ and $v_o(x, y)$, the magnitude and velocity maps, respectively. If these maps are measured with sufficiently high spatial resolution and flow is laminar, one can assume that each voxel contains only one velocity, and therefore the spatial-velocity distribution associated with the object is approximately

$$s(x, y, v) = m(x, y) \times \delta[v - v_o(x, y)], \quad (1)$$

where $\delta(z)$ is the Dirac delta function.

Spiral FVE acquisitions follows a stack-of-spirals pattern in k_x, k_y, k_v space (the k -space associated with the $s(x, y, v)$ distribution) (Fig. 1) [3]. Consequently, k -space data are truncated to a cylinder, i.e., a circle along k_x, k_y (with diameter $1/\Delta r$), and a rectangle along k_v (with width $1/\Delta v$), where Δr and Δv are the prescribed spatial and velocity resolutions, respectively. The associated object domain spatial-velocity blurring can be modeled as a convolution of the true distribution $s(x, y, v)$, with $\text{jinc}\left(\sqrt{x^2 + y^2}/\Delta r\right)$ and $\text{sinc}(v/\Delta v)$, resulting in

$$\hat{s}(x, y, v) = \left[m(x, y) \times \text{sinc}\left(\frac{v - v_o(x, y)}{\Delta v}\right) \right] * \text{jinc}\left(\frac{\sqrt{x^2 + y^2}}{\Delta r}\right) \quad (2)$$

where $\hat{s}(x, y, v)$ is the measured spatial-velocity distribution, $*$ denotes the two-dimensional convolution operation, $\text{sinc}(z) = \sin(\pi z)/(\pi z)$, $\text{jinc}(z) = J_1(\pi z)/(2z)$, and $J_1(z)$ is a Bessel function of the first kind.

2.2. Deconvolution algorithm

Let \mathbf{B} be an image obtained by filtering the original image \mathbf{S} with a point spread function (PSF) \mathbf{J} , and degraded by additive noise ϵ , i.e.:

$$\mathbf{B} = \mathbf{S} * \mathbf{J} + \epsilon. \quad (3)$$

Given the degraded image \mathbf{B} , the PSF \mathbf{J} , and the noise ϵ , recovering the original image \mathbf{S} is a difficult task. This

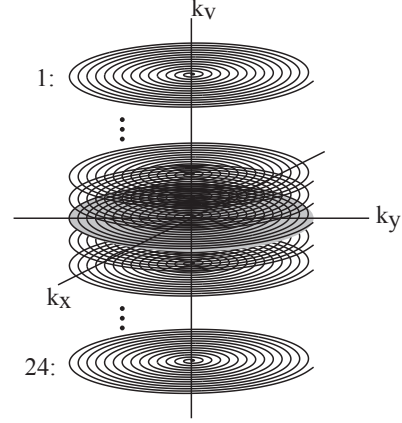


Fig. 1. Spiral FVE acquisitions follows a stack-of-spirals pattern in k_x, k_y, k_v space (the k -space associated with the $s(x, y, v)$ distribution).

problem is called non-blind deconvolution. It is an ill-posed problem, i.e., there may exist more than one image \mathbf{S} that fits Eq.(3).

There are many efficient algorithms and techniques that may be used to find the best approximation of \mathbf{S} that satisfies Eq.(3). We used the deconvolution algorithm recently proposed by Krishnan and Fergus [7]. From a stochastic perspective, this method looks for the maximum *a posteriori* estimate of \mathbf{S} , i.e. from Bayes' theorem we have $p(\mathbf{S}|\mathbf{B}, \mathbf{J}) \propto p(\mathbf{B}|\mathbf{S}, \mathbf{J})p(\mathbf{S})$, and we are interested in the maximum of $p(\mathbf{S}|\mathbf{B}, \mathbf{J})$. Here, the first term is a zero mean Gaussian distribution and the second being a hyper-Laplacian image prior ($p(z) \propto e^{-k|z|^\alpha}$). Maximizing $p(\mathbf{S}|\mathbf{B}, \mathbf{J})$ is equivalent to minimizing the cost function $-\ln p(\mathbf{S}|\mathbf{B}, \mathbf{J})$:

$$\min_{\mathbf{S}} \sum_{i=1}^N \left(\frac{\lambda}{2} (\mathbf{S} * \mathbf{J} - \mathbf{B})_i^2 + |(\mathbf{S} * f_1)_i|^\alpha + |(\mathbf{S} * f_2)_i|^\alpha \right), \quad (4)$$

where i is the pixel index, $*$ is the two dimensional convolution operator and $f_1 = [1 \ -1]$ and $f_2 = [1 \ -1]^T$ are two first-order derivative filters.

Using the half-quadratic penalty method [8], is possible to introduce an auxiliary variable $\mathbf{w} = [w_i^1 \ w_i^2]$ (the numbers j in w_i^j are indices, not power) at each pixel i that allows move the $(\mathbf{S} * f_j)_i$ terms outside the $|\cdot|^\alpha$ expression, giving a new cost function:

$$\min_{\mathbf{S}, \mathbf{w}} \sum_{i=1}^N \left[\frac{\lambda}{2} (\mathbf{S} * \mathbf{J} - \mathbf{B})_i^2 + \frac{\beta}{2} \left(\left\| (\mathbf{S} * f_1)_i - w_i^1 \right\|_2^2 + \left\| (\mathbf{S} * f_2)_i - w_i^2 \right\|_2^2 \right) + |w_i^1|^\alpha + |w_i^2|^\alpha \right] \quad (5)$$

where β is a weight that will vary during the optimization. As $\beta \rightarrow \infty$, the solution of Eq.(5) converges to that in Eq.(4) [8]. Minimizing Eq.(5) for a fixed β is performed alternating

between two steps, in the first step we solve Eq.(5) for S , given a fixed value for w , and in the second step we solve an auxiliary equation for w for fixed S [7].

2.3. Estimating the velocity map

Assuming that the spiral FVE blurred image measured can be written as Eq.(2), then, after deconvolving this image by the PSF $\text{jinc}(r/\Delta r)$, we should obtain

$$\tilde{s}(x, y, v) = m(x, y) \times \text{sinc}\left(\frac{v - v_o(x, y)}{\Delta v}\right), \quad (6)$$

which is a high spatial resolution FVE dataset. Assuming a high-resolution spin-density map, $m(x, y)$, is available (this may be acquired in a separate scan), the velocity v_o associated with a given pixel (x_o, y_o) may be estimated from the $\tilde{s}(x, y, v)$ as

$$\hat{v}(x_o, y_o) = \arg \min_{v_o} \left\| \frac{\tilde{s}(x_o, y_o, v)}{m(x_o, y_o)} - \text{sinc}\left(\frac{v - v_o}{\Delta v}\right) \right\|_2, \quad (7)$$

for $m(x_o, y_o) \neq 0$, otherwise $v_o(x_o, y_o) = 0$.

2.4. Validation

Two sets of experiments were used as a proof-of-concept of the proposed approach.

First, simulated FVE data with 1 mm spatial resolution was derived — using Eq. (2) — from a numerical phantom: a parabolic velocity map, with 0.33 mm spatial resolution ($m(x, y)$ was assumed to be equal to 1 for the entire image). Then, the proposed approach was used estimate the original velocity map. The map estimated from the FVE data was then compared with the original map.

Then, simulated FVE data with 1 mm spatial resolution was derived — using Eq. (2) — from measured phase contrast MRI data: the through-plane velocity map, measured with 0.33 mm spatial resolution, at the carotid bifurcation (in cross-section) of a pulsatile carotid flow phantom (Phantoms by Design, Inc., Bothell, WA) (Fig. 2). Fig. 3 illustrates the difference in spatial resolution between the phase contrast acquisition and the simulated FVE data. A CINE gradient-echo 2DFT phase contrast sequence with high spatial resolution and high SNR (0.33 mm resolution, 10 averages, 80 cm/s Venc) was used to acquire the reference velocity map. The acquisition was prospectively gated, and the following scan parameters were used: 11.6 ms pulse repetition time, 30° flip angle, 3 mm slice profile, and 23.2 ms temporal resolution. The total scan time was 40 minutes. However, the scan time of an FVE acquisition (with scan parameters equivalent to the ones used to generate the simulated data) would be under 1 minute. The proposed approach was used estimate the original velocity map (for this, the high-resolution

magnitude image reconstructed from the phase-contrast data was used as $m(x, y)$). The velocity map estimated from the low-resolution FVE data was then compared with the original high-resolution phase-contrast map.

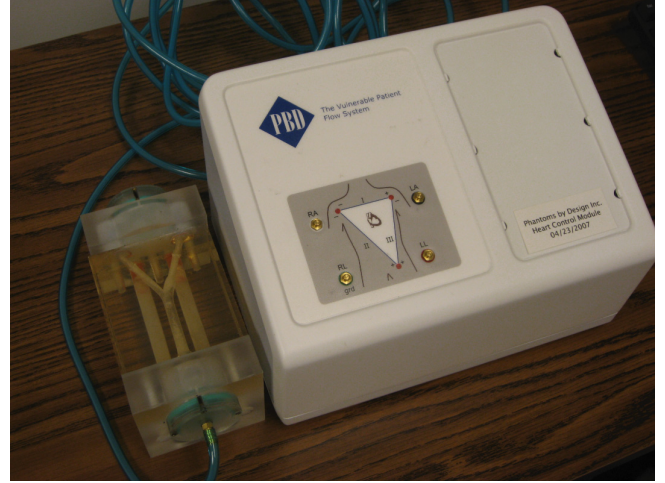


Fig. 2. The pulsatile carotid flow phantom (Phantoms by Design, Inc., Bothell, WA) used to validate the proposed method.

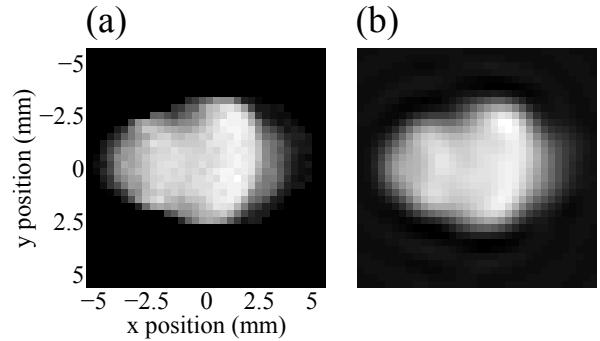


Fig. 3. Magnitude images associated with the cross-section of the phantom's bifurcation, where the phase contrast velocity map was measured: (a) phase contrast data (spatial resolution: 0.33 mm); and (b) FVE data (spatial resolution: 1 mm).

3. RESULTS

Figure 4 presents the results of the validation experiment using the parabolic flow numerical phantom. Spatial deconvolution did not improve reconstruction quality in this experiment, thus we only show the results obtained without spatial deconvolution. The velocity map estimated from the simulated low-resolution FVE data was accurate within 3% for about 85% of the pixels. This is a very important result, as carotid flow distant to the bifurcation — which is typically used as input and output profiles in computational fluid dynamics simulation (CFD) — is typically approximately parabolic. This

means that FVE may potentially be used for modelling CFD simulations of carotid flow, instead of phase contrast. The latter has issues with low SNR and partial volume effects, which are overcome by FVE.

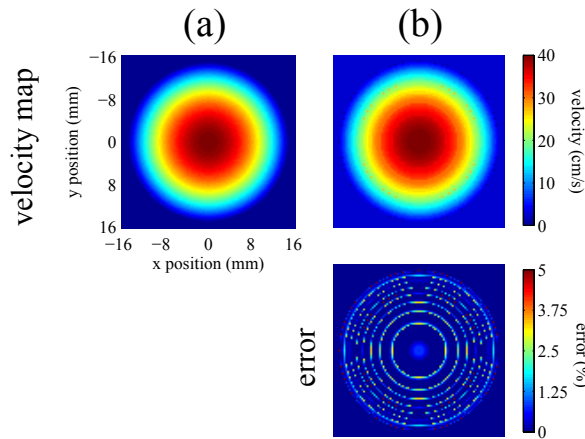


Fig. 4. Validation experiment using a parabolic flow numerical phantom: (a) reference velocity map; (b) velocity map estimated from the simulated low-resolution FVE data, and associated error percentages.

Figure 5 presents the results of the validation experiment using the phase contrast velocity map acquired at the pulsatile carotid flow phantom’s bifurcation. The velocity maps estimated from the simulated low-resolution FVE data are very similar (qualitatively) to the reference map. The error images show that the velocity map obtained using spatial deconvolution (Fig. 5c) was more accurate than the one obtained without spatial deconvolution (Fig. 5b). These good results are also important, as the velocity profile measured at the carotid bifurcation may be used for improving CFD simulation quality [4]. This means that FVE may potentially be used also for driving CFD simulations, with considerably higher SNR and robustness to partial voluming.

4. CONCLUSION

We proposed a method for deriving high-resolution velocity maps from low-resolution FVE measurements. The results showed that it is possible to obtain reasonably accurate velocity maps from the FVE distributions. This suggests that FVE may potentially be used for driving CFD simulations of carotid flow [4], with considerably higher SNR and robustness to partial voluming than phase contrast MRI.

5. REFERENCES

[1] M. O’Donnell, “Nmr blood flow imaging using multi-echo, phase contrast sequences,” *Med Phys*, vol. 12(1), pp. 59–64, 1985.

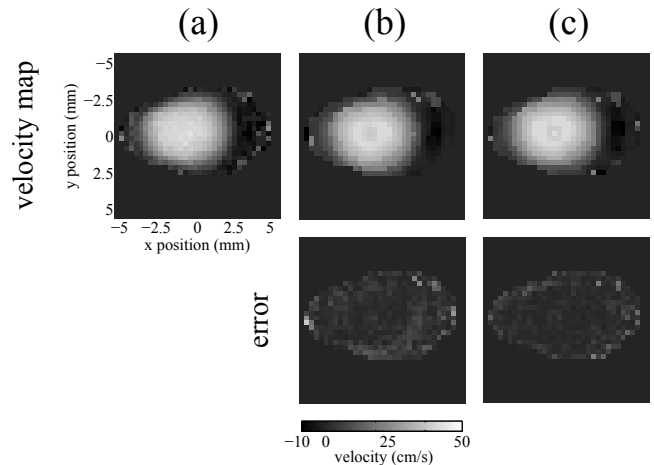


Fig. 5. Validation experiment using a pulsatile carotid flow phantom: (a) reference phase contrast velocity map, measured at the phantom’s bifurcation; (b) velocity map estimated from the simulated low-resolution FVE data, without spatial deconvolution (and associated error percentages); and (c) velocity map estimated from the simulated low-resolution FVE data, with spatial deconvolution (and associated error percentages).

[2] C. Tang, D. D. Blatter, and D. L. Parker, “Accuracy of phase-contrast flow measurements in the presence of partial-volume effects,” *J Magn Reson Imaging*, vol. 3(2), pp. 377–385, 1993.

[3] J. L. A. Carvalho and K. S. Nayak, “Rapid quantitation of cardiovascular flow using slice-selective fourier velocity encoding with spiral readouts,” *Magnetic Resonance in Medicine*, vol. 57, pp. 639–646, 2007.

[4] J.-F. Nielsen and K. S. Nayak, “MR-driven computational fluid dynamics,” in *Proc, ISMRM, 17th Annual Meeting*, Honolulu, 2009, p. 3858.

[5] J. L. A. Carvalho, J. F. Nielsen, and K. S. Nayak, “Feasibility of in vivo measurement of carotid wall shear rate using spiral fourier velocity encoded mri,” *Magnetic Resonance in Medicine*, vol. 63, pp. 1537–1547, 2010.

[6] P. R. Moran, “A flow velocity zeugmatographic interlace for nmr imaging in humans,” *Magn Reson Imaging*, vol. 1, pp. 197–203, 1982.

[7] D. Krishnan and R. Fergus, “Fast image deconvolution using hyper-laplacian priors,” *Neural Information Processing Systems*, 2009.

[8] Y. Wang, J. Yang, W. Yin, and Y. Zhang., “A new alternating minimization algorithm for total variation image reconstruction,” *SIAM J. Imaging Sciences*, vol. 1(3), pp. 248–272, 2008.